Supporting Information

Kimberlin et al. 10.1073/pnas.0910547107

SI Methods

Plasmids and RNA. *Reston* VP35 RBD (residues 160–329) with or without point mutant R301A and *Zaire* VP35 (residues 20–340) with point mutants R305A, K309A, and R312A were subcloned into the pET-46 Ek/LIC vector (Novagen). Point mutations were introduced using the Quikchange II Site-Directed Mutagenesis kit (Stratagene). Deprotected, desalted, duplex synthetic RNA oligos were purchased from Integrated DNA. Sequences are as follows: 18-bp blunt ended (used for crystallization and dot blot assays): sense 5′ AGAAGGAGGGAGGGAGGA 3′; antisense 5′ UCCUCCCUCCCUCCUUCU 3′; 5′ overhang (used for dot blot assays); sense 5′ gagagaaggagggagggagga 3′; antisense 5 ' ctctcctccctccctccttct 3′; 3′ overhang (used for dot blot assays); sense 5′ agaaggagggagggaggagag 3′; antisense 5 ' tcctccctccctccttctctc 3′.

5′ triphosphate–containing RNA oligos were synthesized via in vitro transcription using T7 polymerase and DNA templates. Templates contained a T7 promoter and the desired RNA sequence. Transcription products were chloroform extracted, precipitated, and purified by denaturing PAGE to obtain the desired 18-base RNA oligo with 5′ triphosphate. Sequences are as follows: DNA template: T7 promoter 5′ AATTTAATACGACTCACTATAGG 3′; sense 5′ GGTTCCCTCCCTCCTTCCTATAGTGAGTCGTATTAAATT 3′; antisense 5′ GGAAGGAGGGAGGGAACCTATAGTGAGTCGTATTAAATT 3′.

Expression and Purification. *Reston* and *Zaire* VP35 were expressed in BL21(DE3) *Escherichia coli* cells at 37°C and grown in 1L cultures to an OD600nm of ~0.5. Cells were then induced with 1.5 mM IPTG and incubated at 37°C with shaking at 300 rpm. Expression cultures were harvested and lysed in 20 mM Tris, pH 8.0, 300 mM NaCl, and 10 mM imidazole with the addition of one complete, EDTA-free, protease inhibitor mixture tablet (Roche) using a M-110L Laboratory Microfluidizer (Microfluidics). *Reston* and *Zaire* VP35 were purified via immobilized metal affinity chromatography on Ni-NTA agarose beads (Qiagen) and eluted with lysis buffer + 300 mM imidazole. Purified protein was then dialyzed overnight at 4°C into 25 mM Tris 8.5, 50 mM NaCl, and 2 mM β-mercaptoethanol. Dialyzed protein was further purified by ion exchange and size exclusion chromatography with buffer exchange into storage/crystallization buffer of 10 mM Tris, pH 8.0, 200 mM NaCl, and 5 mM TCEP. Selenomethionine (Se-Met) incorporation was achieved via metabolic inhibition as has been previously described (1).

Dot Blot RNA-Binding Assays. The sense strands of the RNA oligos defined above were end labeled using γ-^{32}P- ATP and T4 polynucleotide kinase (New England Biolabs), purified, and annealed for 5 min at 65°C with anti-sense strands. 5′ triphosphate–capped RNA oligos were body labeled during transcription using α-^{32}P-UTP. Dot blot binding assays were carried out as previously described (2). Briefly, increasing concentrations of purified *Reston* VP35 RBD were incubated in 50 μl reactions with trace amounts of annealed dsRNA in binding buffer (10 mM Tris 7.5, 150 mM NaCl, 6 mM $MgCl_2$, and 2 mM TCEP). Reactions were incubated at room temperature for 1.5 h and then pulled through a dual membrane layer under vacuum using the Minifold I Dot-Blot System vacuum manifold (Whatman). The upper protein-binding membrane was a Protran BA85 (Whatman) and the lower nucleic acid–binding membrane was a Hybond N+ (Amersham). Membranes were removed from the apparatus, dried, and wrapped in plastic wrap. Dried membranes were then exposed overnight to a phosphorscreen (Amersham) and then imaged using a Storm 860 phophorimager (GE Healthcare). Images were quantitated using ImageQuant (GE Healthcare), and data were fit to a modified version of the Hill equation using the Prism software program (GraphPad Software, Inc).

DXMS. To optimize the concentration of guanidine hydrochloride (GuHCl) for best peptide coverage, 10 μL of *Zaire* VP35 (4 mg/mL) was diluted into 30 μL Tris-buffered saline, quenched with 60 μL of 0.8% (vol/vol) formic acid containing various concentrations of GuHCl (0.8, 1.6, 3.2, and 6.4 M) at 0°C, and then frozen at −80°C. The frozen, quenched samples were melted on ice and then immediately passed over an immobilized pepsin column (3, 4), with 0.05% TFA in water at a flow rate of 100 μl/min for 4 min. The duration of digestion was 40 s. The proteolytic products were directly collected by a reverse-phase C18 column and then eluted with a linear 6.4–38.4% acetonitrile gradient over 30 min. The eluate was then transferred to a Finnigan LCQ Classic mass spectrometer (with ion trap) for mass spectrometric analyses, with capillary temperature at 200°C, and with data acquisition in either MS1 profile mode or data-dependent MS/MS mode. The SEQUEST software program (Thermo Finnigan Inc.) was used to identify the sequence of the pepsin-generated peptide ions. This set of peptides was then further examined using DXMS Explorer (5, 6) to obtain peptide coverage maps for various concentrations of GuHCl. The condition with best peptide coverage map was used for deuterium exchange experiments.

Deuterated samples were prepared by adding 10 μL of *Zaire* VP35 stock solution to 30 μL of deuterated buffer (8.3 mM Tris pH7.2, 150 mNaCl) at 0°C. After a 10-s incubation at 0°C, 60 μL 0.8% formic acid and 1.6 M GuHCl were added to quench the H/D exchange reaction, and the samples were stored at −80°C. The deuterated samples were then subjected to the DXMS apparatus described above, along with control samples of nondeuterated and fully deuterated VP35 (incubated in 0.5% formic acid in 100% D_2O for 12 h at room temperature). The centroids of isotopic envelopes of nondeuterated, partially deuterated, and fully deuterated peptides were measured using DXMS Explorer, and then converted to deuteration level with corrections for back-exchange.

SAXS. Small angle x-ray scattering experiments were performed on samples of *Reston* and *Zaire* VP35 prepared in storage buffer + 10% glycerol (added as a free-radical scavenger) at two concentrations each (4.9 and 9.8 mg/mL for *Reston*; 2.3 and 4.0 mg/mL for *Zaire*). Exposures of 0.5 s, 5 s, and a second 0.5 s exposure (to check for radiation damage) of both samples and buffers were collected at beam line 12.3.1 of the Advanced Light Source. Images were circularly averaged, and the scattering from buffer was subtracted with normalization for changes in beam intensity. Molecular weight and oligomerization state were calculated as previously described (7). Briefly, I(0) values extrapolated from the Guinier region of scattering curves were calculated using PRIMUS (8). Molecular weights are calculated by I(o) divided by the protein concentration c, at two different protein concentrations to account for possible concentration-dependent aggregation. I(0)/c values were calculated for both *Reston* and *Zaire* at both concentrations and fitted against a standard curve of I(0)/c values calculated from lysozyme (14 kDa), xylonase (21 kDa), BSA (63 kDa), and glucose isomerase (tetramer of 43 kDa monomers, 172 kDa).

1. Doublié S (1997) Preparation of selenomethionyl proteins for phase determination. *Methods Enzymol* 276:523–530.
2. Wong I, Lohman TM (1993) A double-filter method for nitrocellulose-filter binding: Application to protein-nucleic acid interactions. *Proc Natl Acad Sci USA* 90:5428–5432.
3. Black BE, Brock MA, Bédard S, Woods VL, Jr, Cleveland DW (2007) An epigenetic mark generated by the incorporation of CENP-A into centromeric nucleosomes. *Proc Natl Acad Sci USA* 104:5008–5013.
4. Hsu YH, et al. (2008) Calcium binding rigidifies the C2 domain and the intradomain interaction of GIVA phospholipase A2 as revealed by hydrogen/deuterium exchange mass spectrometry. *J Biol Chem* 283:9820–9827.
5. Black BE, et al. (2004) Structural determinants for generating centromeric chromatin. *Nature* 430:578–582.
6. Burns-Hamuro LL, et al. (2005) Distinct interaction modes of an AKAP bound to two regulatory subunit isoforms of protein kinase A revealed by amide hydrogen/deuterium exchange. *Protein Sci* 14:2982–2992.
7. Putnam CD, Hammel M, Hura GL, Tainer JA (2007) X-ray solution scattering (SAXS) combined with crystallography and computation: Defining accurate macromolecular structures, conformations and assemblies in solution. *Q Rev Biophys* 40:191–285.
8. Konarev PV, Volchkov VV, Sokolova AV, Koch MHJ, Svergun DI (2003) PRIMUS: A Windowed PC-based system for small-angle scattering data analysis. *J Appl Cryst* 36:1277–1282. Q:1

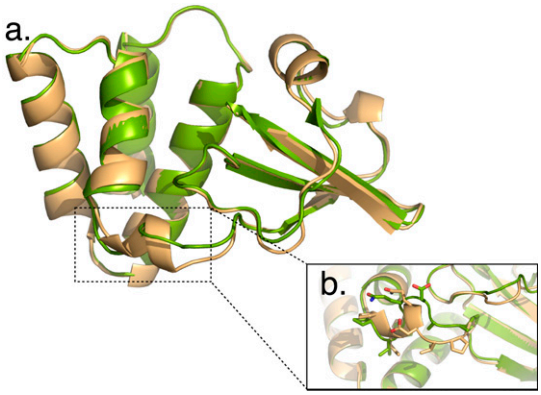

Fig. S1. *Reston* and *Zaire* VP35 RBDs are highly similar. (*a*) Structural alignment of *Reston* VP35 RBD (orange) with *Zaire* VP35 RBD (green, PDB ID: 3FKE) gives an overall RMSD of 0.7 Å^2 showing a conservation of molecular architecture. (*b*) The only significant structural difference between species lies in residues 274–281 (Reston numbering), which forms the small fifth helix in the Reston structure but forms a loop in the Zaire structure.

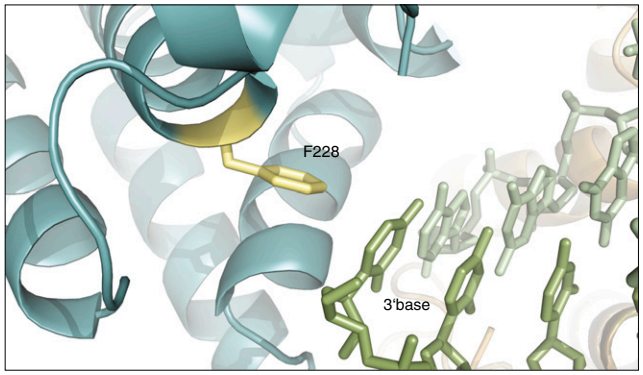

Fig. S2. Residue F228 of *Reston* VP35 forms a herringbone structure, arranged perpendicularly to the ring of the 3′ terminal nitrogen base of the dsRNA.

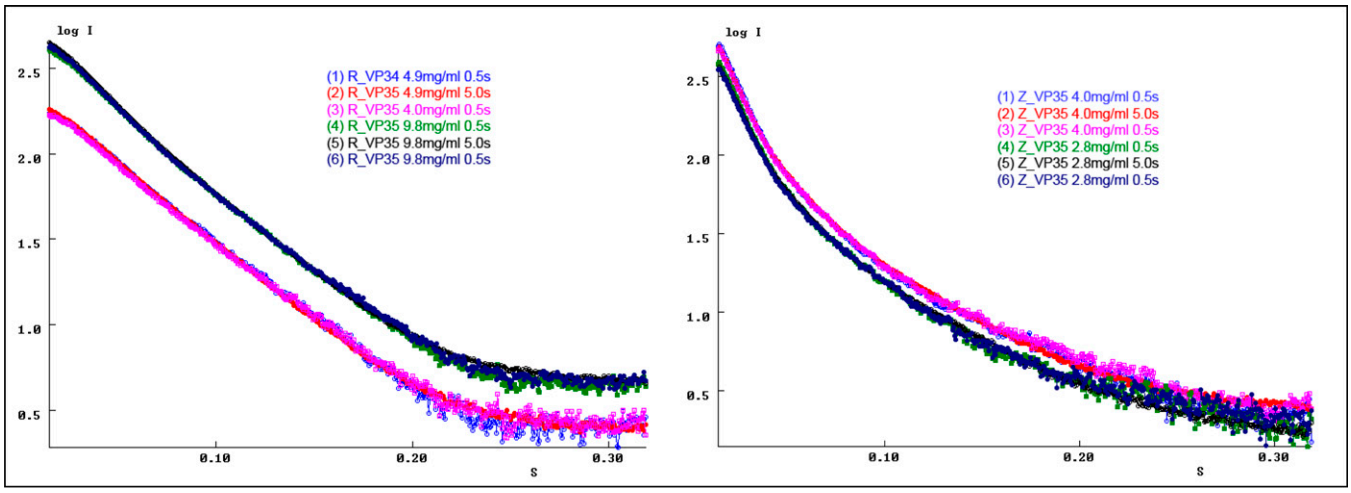

Fig. S3. Raw SAXS data. Circularly averaged scattering profiles for both *Reston* VP35 RBD (R_VP35, left) and *Zaire* VP35 (Z_VP35, right) at two different concentrations with short (0.5 s) and long (5.0 s) exposures.

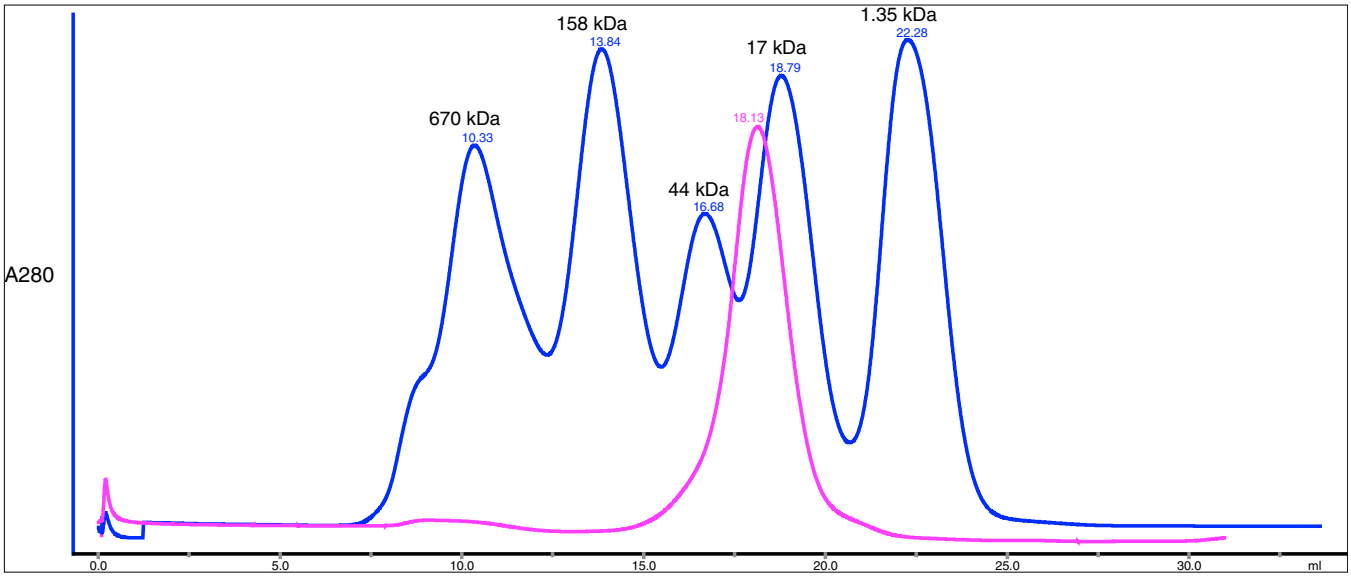

Fig. S4. Gel filtration profile of the *Reston* VP35 RBD on a Superdex 200 10/300 GL overlaid with a gel filtration standard (Biorad). Retention volume suggests a hydrodynamic volume consistent with a monomeric form of the RBD in the absence of dsRNA.

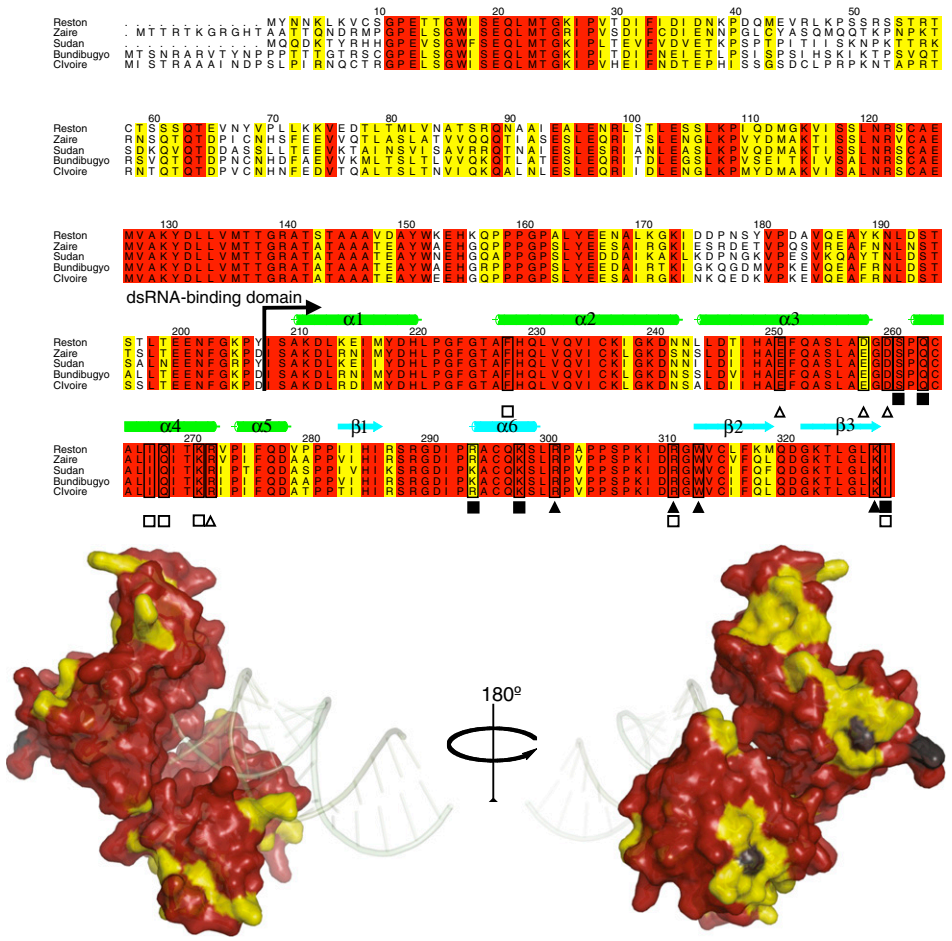

Q:2 **Fig. S5.** Sequence alignment of VP35 from all five species of *ebolavirus*. Secondary structural elements observed for the dsRNA-binding domain are indicated, with α-helical domain in green and β-sheet domain in blue. Residues involved in the dimer interface (backbone binding, closed triangles; end-capping, open triangles) and in RNA binding (backbone-binding, closed squares; end-capping, open squares) are highlighted. Structure of the dimeric RBD in complex with dsRNA is shown below. Amino acids that are identical among Reston, Zaire, Sudan, Côte d'Ivoire, and Bundibugyo and are colored red; amino acids that are similar are colored yellow; amino acids that differ significantly are colored black. Regions involved in dsRNA binding and dimer formation are conserved (red), except for the relatively conservative substitutions D258E and R294K (Reston numbering) between *Reston* and *Zaire*. Position 258 lies in the dimer interface. It is possible that the shorter length of the D253 side chain in *Reston*, as compared with E253 in *Zaire*, could lead to weaker hydrogen bonding between monomers and perhaps less significant cooperativity in dsRNA recognition and sequestration. However, it is not yet known whether these two substitutions confer any phenotypic difference to the two species of *ebolavirus*.

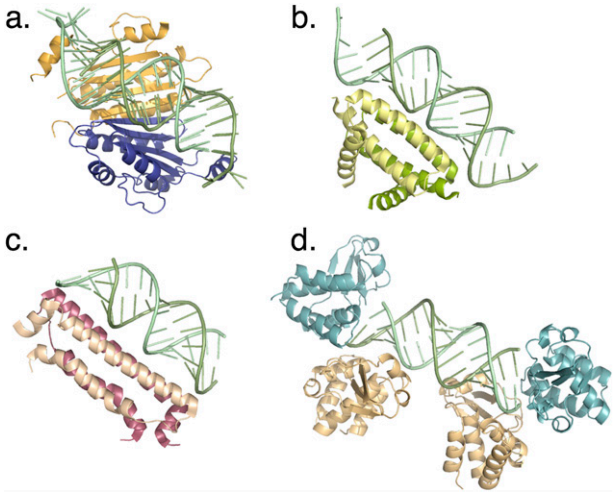

Fig. S6. Four unique examples of viral dsRNA-binding proteins in complex with dsRNA. (*a*) *Tombavirus* P19 (PDB code 1RPU) forms an extensive dimer interface at the center of the dsRNA complex while also capping the ends. (*b*) Dimeric influenza virus NS1 (PDB code 2ZKO) binds along the phosphate backbone only and does not cap the terminal ends of the dsRNA. (*c*) Dimeric Flock House virus B2 (PDB code 2AZ0) similarly binds along the dsRNA backbone, allowing the protein to coat the dsRNA. (*d*) *Reston ebolavirus* VP35 forms backbone-binding and end-capping interactions. Note that each viral protein dimerizes to recognize dsRNA. *Ebolavirus* VP35 binds to both the end and the end-proximal backbone of the dsRNA oligo but appears to be insensitive to oligo length. Because VP35 binds the ends, the number of VP35s that could attach to any given dsRNA molecule is limited. By contrast, Flock House virus B2 and influenza NS1 bind only the backbone, not the ends, hence, any number of B2 or NS1 molecules could coat the backbone, depending on the length of the dsRNA molecule. Like VP35, *Tombusvirus* P19 forms a dimer and caps the dsRNA ends. However, only one P19 monomer binds each end of the dsRNA oligo, with the two members of the P19 dimer meeting in the middle of the dsRNA–protein complex. Thus, the length of oligo recognizable by P19 is limited by the fixed span of the P19 dimer. By contrast, VP35 appears insensitive to dsRNA length, as the VP35 dimer on one end of the dsRNA forms no contact with the dimer on the other end. Each of these viruses has evolved a unique structural mechanism for binding dsRNA, creating a palette of possibilities by which a virus may silence and sequester this pathogen-associated molecular pattern.

Table S1. Data collection, phasing, and refinement statistics

Data collection	SeMet unbound	Native unbound	Native dsRNA bound
Space group	R32	R32	$P3_1$
Cell dimensions			
a, *b*, *c* (Å)	158.3,158.3,167.2	158.3,158.3,167.2	85.6, 85.6, 108.8
α, β, γ (°)	90, 90, 120	90, 90, 120	90, 90, 120
Wavelength	0.9793	0.9793	0.9795
Resolution (Å)	47.57–3.25 (3.37–3.25)	45.66–2.40 (2.49–2.40)	37.08–2.28 (2.38–2.28)
R_{sym} or R_{merge}	0.134 (0.484)	0.080 (0.544)	0.061 (0.254)
I / σI	6.3 (1.9)	9.4 (2.0)	23.47 (5.03)
Completeness (%)	99.5 (9.4)	96.1 (97.9)	81.4 (35.5)*
Redundancy	3.71 (3.52)	5.69 (5.65)	4.3 (1.43)
Refinement			
Resolution (Å)		45.66–2.40 (2.49–2.40)	37.08–2.40 (2.49–2.40)
No. reflections		30140	29669
R_{work} / R_{free}		0.198 / 0.219	0.198 / 0.239
No. atoms			
Protein		1,949	3846
Ligand/ion		n/a	761
Water		82	150
B-factors			
Protein		55.46	40.59
Ligand/ion		n/a	54.44
Water		60.41	38.60
RMS deviations			
Bond lengths (Å)		0.008	0.021
Bond angles (°)		1.020	1.304

Values in parentheses are for highest-resolution shell.

*Low completeness in high-resolution shells is caused by strong anisotropic diffraction of the crystals.